S&V Geometry 101

George Fox Lang, Data Physics Corporation, San Jose, California

Vibration analysis of rotating machinery is a proven means of detecting flaws and degradation. To get the maximum return from such an effort, you must understand how the geometric interplay of machine components determines the noise and vibration spectra that will be exhibited. This article is intended as an introduction-to-topic for the new diagnostician; it discusses gears and bearings, essential elements that can introduce dominant peaks in a machine spectrum.

We will review the determination of certain frequencies at which oscillating operating forces are developed in simple machine elements. We will also discuss why signature spectra may contain sums and differences of such frequencies in addition to the more obvious harmonic multiples. Basic "tools of the trade" will be reviewed and demonstrated by example.

Be Prepared to be Surprised . . . Have a Shopping List

Even seemingly simple machines can exhibit relatively complex spectra with a myriad of peaks attributable to several different physical mechanisms. In order to decipher what the machine is trying to tell you, it is necessary to perform some simple geometric analysis *before* embarking on field measurements. You owe it to yourself to prepare a list of frequencies that you *expect* to dominate the signatures. Then, when an *unexpected* component enters the picture, you are prepared to recognize it as such.

We will examine some measurements from the small machine shown in Figure 1. This is a tiny two-stage gear reduction box driven by a six-pole DC motor. It is incorporated in one of those fiendish devices that snatches your hard-earned dollar, subjects it to rude inspection and rewards you with a handful of "pocket anchors." The two gear-like wheels visible in this photo drive a pair of soft rubber Gilmer belts used to suck your banknote into a slot (and often to reject it rudely in protest of your billfold maintenance program).

The internal workings of this drive are shown schematically in Figure 2. A small spur gear mounted on the motor shaft drives a larger gear on an intermediate shaft. This transfer shaft also spins a worm gear, which engages a mating helical spur mounted to the output shaft. The axis of the output shaft is thus perpendicular to the axes of the motor and transfer shafts.

Hence our machine is characterized by three shafts and two gear meshes. Each of these elements influences the nature of the machine's vibration. To understand measurements made from the machine, we need to understand the details of its geometry. In the main, this simply means that repetitive elements such as gear teeth must be counted. This sounds like a simple task, but when drawings are not available it can be a time consuming nuisance. Still, without these basic facts, you will not be "qualified to be surprised" by the dynamics of the machine you must diagnose.

Table 1 illustrates the start of a "shopping list" for the bill changer. This list contains the speeds of the shafts, the expected "mesh" frequencies and various "fault mechanism" frequencies including such items as the contact rate between motor brushes and commutator segments. Knowing the geometry of the machine allows us to determine these frequencies *relative to the turning speed of one shaft*. In our example, the transfer shaft turns 10/23 as fast as the motor and the output shaft rotates at 1/16 of this speed. Normally, the *output* shaft is used as the reference as the typical operating speed of this shaft is most frequently known. The relative speeds shown in Table 1 are normalized with respect to the output shaft.

Multiplying the relative speeds by the rotational rate of the reference shaft allows a list of anticipated dominant frequencies to be written for a single operating point. This is directly useful information for a constant-speed machine. When a vari-

Figure 1: Our test object is the drive mechanism for a currency bill exchanger, a two-stage 36.8:1 reduction gear-train powered by a small DC motor.

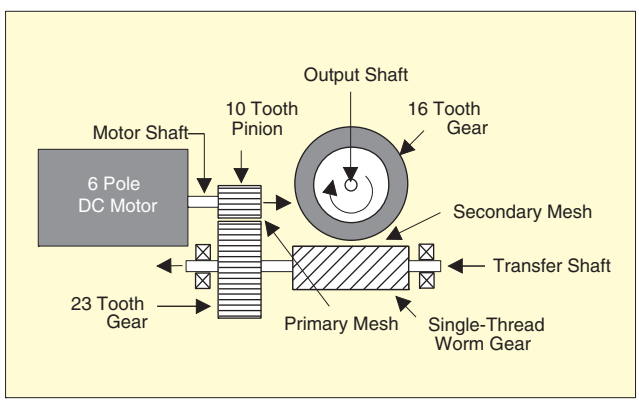

Figure 2: Schematic diagram of currency bill exchanger shows three shafts and two stages of gear reduction. Pertinent geometric features are noted.

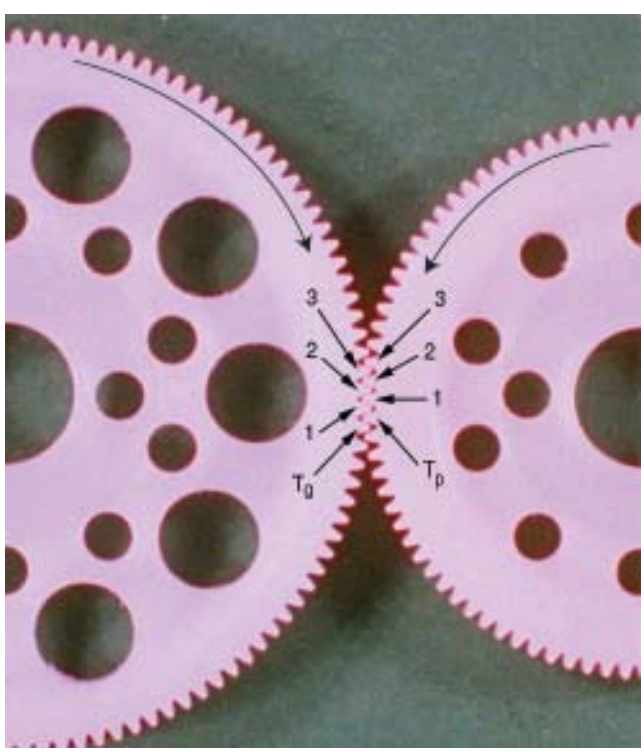

Figure 3. Tooth numbering convention shown on two spur gears.

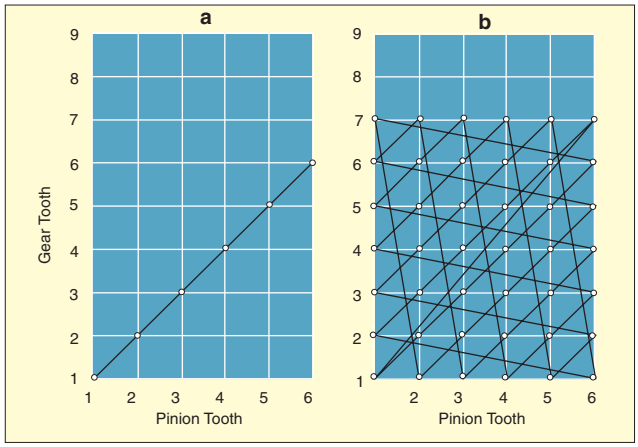

Figure 4. (a) Tooth-mating sequence between 6-tooth gear and 6-tooth pinion. Note that only like-numbered teeth enter mesh together. (b) Tooth-mating sequence between 6-tooth pinion and 7-tooth gear. Note each pinion tooth meshes with every gear tooth and viceversa.

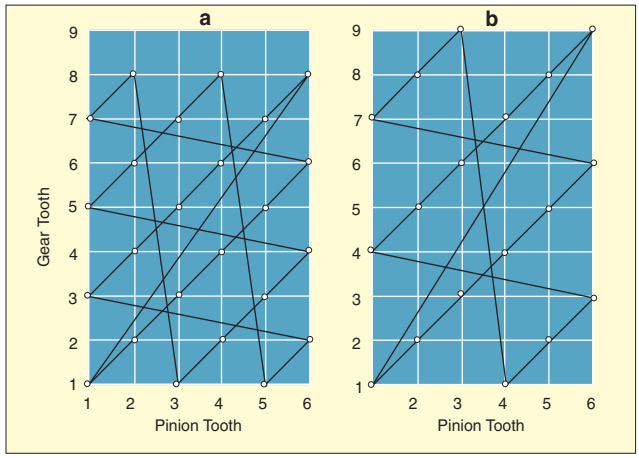

Figure 5. (a) Tooth-mating sequence between 6-tooth pinion and 8-tooth gear. Note that each pinion tooth meshes with only four gear teeth; each gear tooth engages only three pinion teeth. (b) Tooth-mating sequence between a 6-tooth pinion and 9-tooth gear. Note that each pinion tooth meshes with three gear teeth; each gear tooth meshes with two pinion teeth.

able speed situation is encountered, it is wise to evaluate this list at the extremes of the speed range; this defines the frequency span and resolution required to study the machine at any speed within its range.

We will depart from this example for a short while to derive some of the typical entries that appear on such shopping lists. And we shall return to this machine for some experimental exhibits.

Some Necessary Dental Work

The most important step in any gear analysis is to count the teeth on every gear. This not only allows you to determine "shopping list frequencies," it allows you to *determine if the signature spectra are likely to change simply because the machine was disassembled* and reassembled without marking engaging gears. You can also determine whether *sub-harmonics* of certain frequencies are likely to appear in the spectra.

Figure 3 shows the engagement of two small *spur* gears. By convention, the smaller of these is termed the *pinion*, the larger the *gear*. The *gear ratio* (more properly, the *gear reduction ratio*) is simply the number of teeth on the gear T_g divided by the number of pinion teeth T_p. Clearly, the speed of the pinion shaft must always be equal to the speed of the gear shaft multiplied by this ratio and the torque carried by the pinion shaft is (essentially) equal to that carried by the gear shaft divided by the gear ratio. The same "laws" govern the mating of two *bevel* gears; the sole difference is that the axes of the pinion and gear shafts are perpendicular rather than parallel.

But, T_g and T_p tell us far more than the speed and torque ratio. Note the tooth numbering illustrated in Figure 3. The teeth of both elements are numbered in the sequence of engagement starting from the current point of mesh. Consider the pattern of tooth engagement that occurs as the gears turn. Figures 4 and 5 illustrate such patterns for sets of slightly different ratios.

In Figure 4a, two identical 6-tooth gears are rotated. On every rotation, like-numbered teeth enter the mesh. Hence, pinion tooth 3 always conveys its load to gear tooth 3, and so on. Since like-numbered gear and pinion tooth-pairs are mated throughout their service life, it is likely that they will develop complimentary wear patterns to compensate for any minute imperfections of manufacture or installation. Should this gear pair be separated during a repair, *the odds are 5 to 1 that this same arrangement of parts will not be restored* unless the mating teeth are marked at disassembly. In subsequent operation, the mating teeth will no longer have their hard-won complimentary wear patterns; this can cause a signature change.

Figure 4b illustrates an entirely different situation. Here, a 6-tooth pinion drives a 7-tooth gear. Note that every pinion tooth eventually drives every gear tooth. All 42 possible tooth-

Table 1. An initial "shopping list" for the currency exchanger generated from the schematic geometry.

Item	Relative Speed	Operating Speed (Hz)	
Shafts		125 RPM	160 RPM
Output	1	2.08	2.67
Transfer	16	33.28	42.67
Motor	36.8	76.67	98.13
Gear Meshes			
Secondary (high speed) Mesh	16	33.28	42.67
Assembly Pass	16	33.28	42.67
Hunting Tooth	1	2.08	2.67
Primary (low speed) Mesh	368	766.67	981.33
Assembly Pass	368	766.67	981.33
Hunting Tooth	1.60	3.33	4.27
Gear Faults			
Eccentric Motor Pinion	368 ±36.8 = 331.2, 404.8	690.00, 841.98	883.20, 1080.82
Eccentric Transfer Gear	368 ±16 = 352, 384	733.33, 800.00	938.67, 1024.00
Eccentric Transfer Worm	16 ±16 = 0, 32	0.00, 66.67	0.00, 85.33
Eccentric Output Gear	16 ±1 = 15, 17	31.25, 35.42	40.00, 45.33
Other Faults			
Magnetic Pole-Pass	6× Motor Shaft = 220.8	460.00	588.80
Brush/Segment Contact	12× Motor Shaft = 441.6	920.00	1177.60

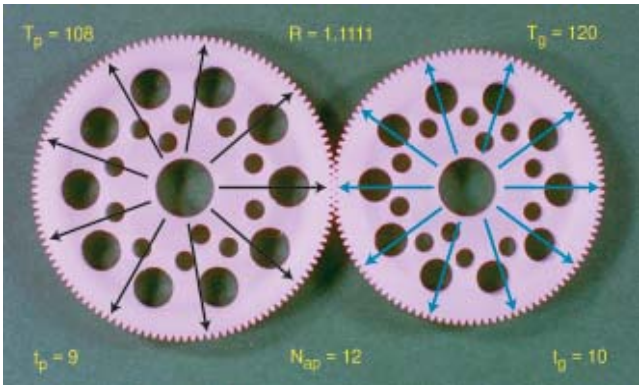

Figure 6. Mesh on a 108-tooth pinion and 120-tooth gear exhibits 12 assembly phases. The teeth of one assembly phase are marked.

mating combinations are encountered in seven pinion revolutions (six gear revolutions). That is, this gear set can only be assembled in one way and there is no benefit to marking its components at disassembly. Such a gear set is said to have one *assembly phase* in contrast to the set of Figure 4a, which has six assembly phases.

Figure 5 shows two examples between these extremes. In Figure 5a, a 6-tooth pinion drives an 8-tooth gear. Note that every pinion tooth comes into mesh with only four gear teeth. Every gear tooth mates with exactly three pinion teeth. In short, this gear-set has two assembly phases. By following the path lines between tooth-pair intersection points, you will note that a given pair of teeth enters the mesh once every 3 gear rotations (every 4 pinion rotations).

Figure 5b presents a gear-set with three assembly phases. Here, a 6-tooth pinion mates with a 9-tooth gear. Each pinion tooth engages three gear teeth while each gear tooth enters mesh with either of two pinion teeth. A given pair of teeth enters the mesh every 2 gear rotations corresponding to 3 pinion rotations.

We can summarize these important observations in a few useful equations. Equation (1) is the key to understanding the gear set. N_{ap} is the largest common (integer) factor contained in both T_p and T_g. Thus for the 6:6 set of Figure 4a, N_{ap} equals 6. For the 6:7 set of Figure 4b, N_{ap} equals 1. The 6:8 set of Figure 5a has a N_{ap} of 2, while the 6:9 set of Figure 5b has an N_{ap} of 3. This common factor is equal to the number of assembly phases between the gears.

$$R = \frac{T_g}{T_p} = \frac{N_{ap} t_g}{N_{ap} t_p} \tag{1}$$

where:

R = the gear reduction ratio
T_g = the number of teeth on the gear
T_p = the number of teeth on the pinion
N_{ap} = the number of assembly phases for the gear set . . . numerically equal to the highest (integer) common factor between T_g and T_p
t_g = the number of gear teeth per assembly phase
t_p = the number of pinion teeth per assembly phase

Figure 6 illustrates one of the twelve (N_{ap}) possible assembly phases of a 108:120 gear set. The 9 pinion teeth (t_p) and 10 gear teeth (t_g) in this phase are marked. While all of the pinion and gear teeth participate in mesh, any tooth within this phase can only contact the mates shown. Clearly, this gear-pair may be assembled with twelve different tooth-mating sequences.

Worm drives are characterized by the same equations. Rather than counting teeth, we need to determine the number of parallel screwlike threads on the pinion; this integer is used as T_p. Figure 7 illustrates the second-stage reduction in our bill-changer, a single-thread ($T_p = t_p = 1$) design.

The frequencies defined by Equations (2) through (6) can all be expected to be present (with varying intensities) in any gearing signature. Invariably, f_{mesh} will be a dominant component in any noise or vibration spectrum measured from a gearbox. Note that gear mesh is a much higher frequency than the shaft

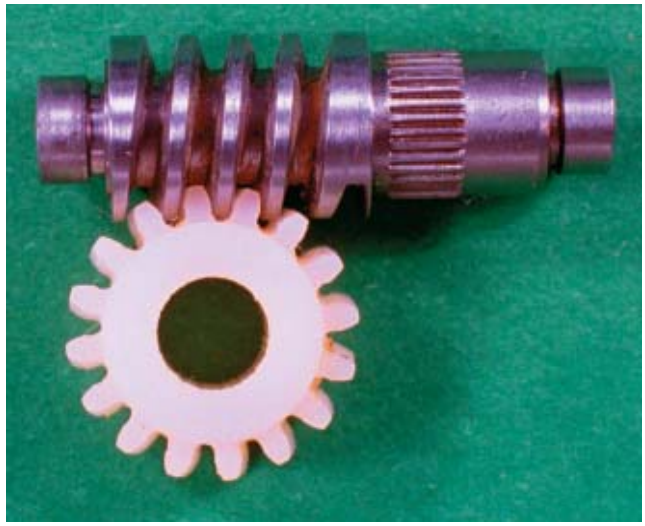

Figure 7. Mesh between a worm pinion and spur gear. The equivalent tooth-count for the worm is equal to the number of parallel threads (one, in this case) cut upon it.

speeds, the assembly phase passage frequency and the "hunting tooth" frequency. In fact, all of these frequencies are *integer subharmonics* of f_{mesh}. The hunting-tooth frequency is the lowest characteristic frequency of the gear-pair and the remaining characteristic frequencies are *integer harmonics* of $f_{\text{hunting tooth}}$.

$$f_{\text{gear}} = \frac{\text{RPM}_{\text{gear}}}{60} \tag{2}$$

where:

RPM_{gear} = the gear-shaft turning speed in RPM
f_{gear} = the (same) gear-turning frequency in Hertz

$$f_{\text{pinion}} = R\, f_{\text{gear}} \tag{3}$$

where:

f_{pinion} = the turning speed of the pinion shaft in Hertz

$$f_{\text{mesh}} = T_g f_{\text{gear}} = T_p f_{\text{pinion}} \tag{4}$$

where:

f_{mesh} = the frequency at which teeth-pairs enter the gear mesh

$$f_{\text{assembly pass}} = t_g f_{\text{gear}} = t_p f_{\text{pinion}} = \frac{f_{\text{mesh}}}{N_{ap}} \tag{5}$$

where:

$f_{\text{assembly pass}}$ = the frequency at which an *assembly phase* passes through mesh

$$f_{\text{hunting tooth}} = \frac{f_{\text{gear}}}{t_p} = \frac{f_{\text{pinion}}}{t_g} = \frac{f_{\text{mesh}}}{N_{ap} t_g t_p} = \frac{N_{ap} f_{\text{mesh}}}{T_g T_p} \tag{6}$$

where:

$f_{\text{hunting tooth}}$ = the frequency at which a *specific tooth pair* mates in mesh

Gears function to transmit torque from one shaft to another. If this were a perfect world, they would do so with the quiet smoothness of a pair of rolling elements in perfect contact with infinite friction at their juncture. Tooth profiles are carefully designed to pass load from one tooth to the next as smoothly as possible. They engage one another with an intended rolling contact and as little sliding as possible to preserve high efficiency. Unfortunately, perfection has eluded us and real gears perform this load hand-off between adjacent tooth-pairs with a certain amount of impacting, sliding, bending and other socially undesirable behavior.

This "mating activity" repeats at the mesh frequency. f_{mesh} and its harmonics are always present in the noise and vibration spectra, most particularly when the gears are lightly loaded. Because the torque transfer is affected as a force transfer at a radial distance from the shaft axes, these events are detectable in translational measurements in the case of the

machine.

The remaining characteristic frequencies, $f_{\text{hunting tooth}}$, f_{gear}, f_{pinion} and f_{assembly} pass are normally less evident in a smooth gear-set. The shaft speeds f_{gear} and f_{pinion} may appear in vibration spectra due to unbalance of the driver or driven element. Second harmonics of these terms often accompany misalignment of shafting (or loose mounting of a drivetrain component). Generally, these frequencies indicate problems external to the gear-set.

In contrast, a small eccentricity of the pinion on its shaft will induce vibration at the *sum and difference frequencies*, $f_{\text{mesh}} + f_{\text{pinion}}$ and $f_{\text{mesh}} - f_{\text{pinion}}$, while a similar problem with the gear will produce detectable activity at $f_{\text{mesh}} + f_{\text{pinion}}$ and $f_{\text{mesh}} - f_{\text{pinion}}$. In general, the amplitude exhibited at a "sum frequency" will be (about) equal to that at the corresponding "difference frequency." That is, the eccentricity signatures exhibit symmetric sidebands about the mesh frequency. This behavior comes about because the shaft-frequency eccentricity modulates the amplitude of dynamic forces present in the mesh.

Amplitude modulation involves a time-domain multiplication. For simplicity, assume that a "normal" acceleration signature initially contains a "gear mesh" component in response to the sinusoidal force:

$$F(t) = F\cos(2\pi f_{\text{mesh}}\, t) \tag{7}$$

Further assume that the gear then becomes slightly eccentric on its shaft and that the "normalized" degree of its deviation from uniform contact at the mesh point can be expressed as:

$$m(t) = e\cos(2\pi f_{\text{gear}}\, t) \tag{8}$$

The dynamic mesh force then becomes:

$$\begin{aligned} F'(t) &= [1 + m(t)]\cdot F(t) = [1 + \mathrm{e}\cos(2\pi f_{\text{gear}} t)]\cdot F\cos(2\pi f_{\text{mesh}} t) \\ &= \frac{\mathrm{e}}{2} F\cos[2\pi(f_{mesh} - f_{\text{gear}})t] + F\cos(2\pi f_{\text{mesh}} t) \\ &\quad + \frac{\mathrm{e}}{2} F\cos[2\pi(f_{mesh} + f_{\text{gear}})t] \end{aligned} \tag{9}$$

This model is simplistic, but it makes the telling point that time-domain multiplication of two sinusoids gives rise to equal-amplitude sinusoids at the sum and difference frequencies. In practice, both the mesh frequency *carrier* and the gear-shaft frequency *modulator* can have many harmonics (of various phasing) present. This means that the resulting modulated signal can be more complicated with distinct tones appearing at frequencies of $nf_{\text{mesh}} \pm kf_{\text{gear}}$, where n and k are integer constants. Normally, the terms symmetrically disposed about f_{mesh} (where n equals 1) will dominate. Sidebands associated with low k value are usually the most detectable. (But, remember resonances and "being prepared to be surprised?")

Gear wear and clearance changes in plain bearings can cause a change in the f_{gear} and f_{pinion} sidebands. So can an unrelated repair that causes the gears to be re-mated with "new" Assembly Phasing. Such unintended signature change may also be accompanied by a rise in the $\pm f_{\text{assembly pass}}$ sidebands of f_{mesh} and its harmonics (when these terms are unique).

In a 1:1 gearing, $N_{ap} = T_p = T_g$, so that $t_p = t_g = 1$. Hence, $f_{\text{assembly pass}} = f_{\text{gear}} = f_{\text{pinion}}$ and the assembly phase passage frequency is not a unique characteristic.

When the gear-set is *designed for uniform distribution of tooth wear*, the gear and pinion tooth-counts share no prime numbers in common, save 1. In this circumstance, $N_{ap} = 1$, resulting in $f_{\text{assembly pass}} = f_{\text{mesh}}$. Hence any $\pm f_{\text{assembly pass}}$ sidebands of f_{mesh} and its harmonics will appear as either an harmonic of f_{mesh} or at DC; they will not be uniquely identifiable.

In all other situations, $f_{\text{assembly pass}}$ is a unique characteristic frequency. Since $f_{\text{assembly pass}}$ is typically much higher than either f_{gear} or f_{pinion}, the $\pm f_{\text{assembly pass}}$ sidebands of f_{mesh} will be widely spaced from their carrier and are not likely to be confused as "high k" images of either f_{gear} or f_{pinion}.

The very low frequency $f_{\text{hunting tooth}}$ is a clear indicator of severe local tooth-pair damage such as that encountered when the mesh has "digested" a significant solid contaminant. This term also shows up as a pair of symmetric sidebands centered upon the mesh frequency. It is difficult to detect these $f_{\text{mesh}} \pm f_{\text{hunting tooth}}$ components and differentiates them from gear mesh (particularly in *uniform tooth wear* gearing) owing to the close frequency spacing. An *order normalized* analysis of *at least* $T_g T_p / N_{ap}$ lines of spectral resolution is required to detect these indicators. They are worth separating; when they are observed, they typically *indicate local tooth damage that can be seen with the unaided eye.*

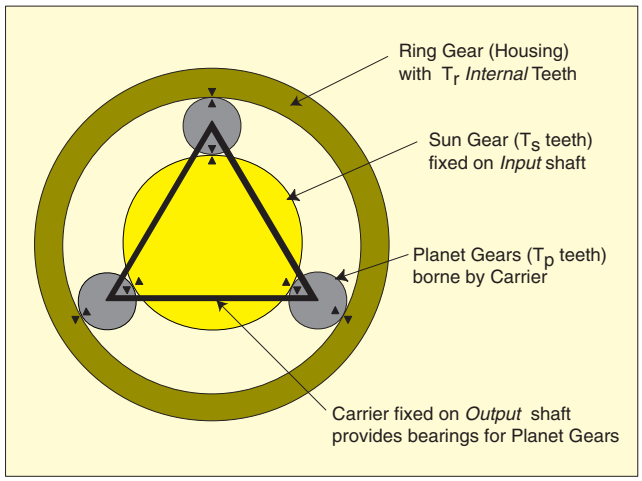

Figure 8. Elements of a simple planetary or epicyclic gear train. In this example, the input shaft turns the Sun Gear while the output shaft turns with the Carrier that provides bearings for the multiple (identical) Planet Gears. The stationary housing is an internally toothed Ring Gear. Many other configurations using spur and bevel gears are possible.

Of Gears and Astronomy

The preceding figures have shown the simplest of gear interplays, the basic stepping stone of which complex gear systems may be built. Such systems are frequently discussed in the literature of our business. There exists another class of gearing that is less frequently discussed, one that is particularly elegant in its geometric arrangement and functional capability: the *planetary* or *epicyclic* gear train. These systems incorporate an additional rotational degree-of-freedom with several benefits in reward for the added complexity.

Planetary systems can provide reduction ratios in excess of component tooth ratios, permitting more compact reduction systems. They can permit output torque sharing between two shafts running at instantaneously different speeds (as in an automobile differential). They can facilitate input load sharing from two or more asynchronous engines (as in a helicopter transmission). The additional DOF can be controlled by a cam to derive a prescribed periodic rotary motion from a constant speed source (as in a commercial movie projector).

Figure 8 illustrates the schematic of a very basic epicyclic speed-reducer. In this system, the innermost *Sun* gear is driven by the input shaft. A series of identical *planet* gears engage the *Sun* gear and an internal *ring* gear cut into the stationary housing. The Output shaft is affixed to the *carrier*, a rotating structure that provides the bearings for the planets. When the Sun gear rotates, the carrier revolves in the same direction at a much-reduced speed. The planet gears spin (with opposite sense) about their own axes and precess with the *carrier*.

The motion of such a system can best be understood by a *superposition analysis* utilizing a sequence of *two* simple motional inputs as shown in Figure 9. First, the carrier is "locked" in position and the housing ring is "freed" to rotate; the planet gears are rotated through an arbitrary angle, say β. In response to this input, the Sun and ring gears revolve in opposite directions. Second, all elements of the gear train are "locked" together and the entire assembly is rotated backwards as a "rigid body" until the housing ring gear is in its original position. The positions of all elements are now identical to those that would

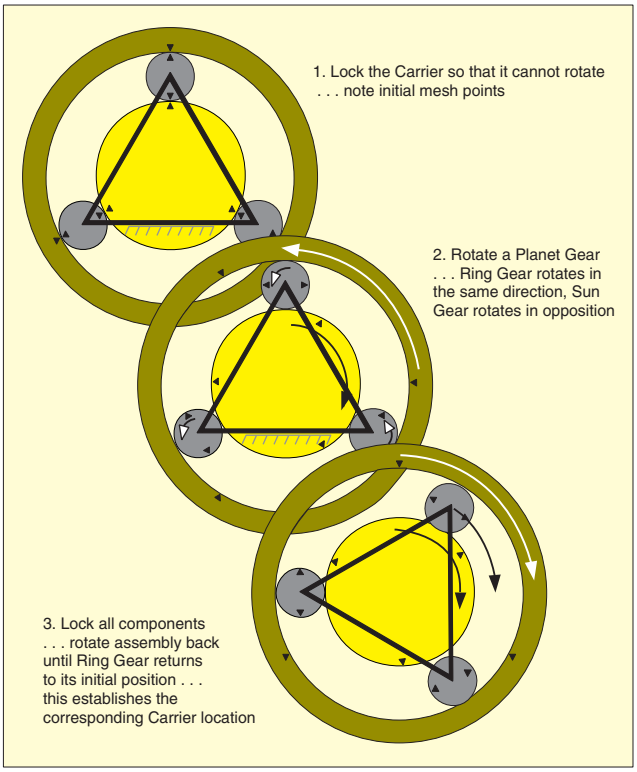

Figure 9.Visualizing epicyclic behavior through the superposition of two motional inputs. First the relative "mesh motions" are input while allowing the housing to rotate; then the housing is returned to its proper stationary position. Absolute rotations are thus seen as the sum of two relative rotations, only one of which involves gear-mesh activity.

have resulted from leaving the ring in its normal "stationary" position and rotating the input shaft until the planets had spun through the angle β *relative* to the Sun and ring gears.

Table 2 presents a tabular analysis of these actions. In the first row, the rotational effects of the "solar" rotation of a planet are provided for all elements. In the second row, the "sidereal" rotations of all elements needed to return the housing to its proper location are listed. The third row contains the sum of these two actions and provides the total rotations of all components at the completion of the second input. The second column describes the input shaft, the third the output shaft.

These tabular results are repeated in Table 3, but are normalized by dividing all entries by the output shaft (carrier) rotation. That is, the rotations of all components are presented for one revolution of the output shaft. From these entries we can discern:

$$R = \frac{\text{Input Rotation}}{\text{Output Rotation}} = 1 + \frac{T_r}{T_s} = \frac{f_{\text{in}}}{f_{\text{out}}} \tag{10}$$

Since the second step "corrective rotation" of the housing does not involve the gear meshing in any way, we further recognize the relationship between the spin frequency of the planet gears and the output shaft speed to be:

$$f_{\text{spin}} = -\frac{T_r}{T_p} f_{\text{out}} \tag{11}$$

The negative sign in (11) indicates that the planets spin in the opposite direction from the Sun gear rotation and carrier precession. The gear mesh frequency is simply the number of planet gear teeth multiplied by the planet spin frequency and we may state:

$$f_{\text{mesh}} = T_r f_{\text{out}} \tag{12}$$

Note that both the ring/planet and planet/Sun meshes occur at the *same* frequency. Other planetary configurations utilizing only spur or bevel gears (but no ring gear) are possible and these can exhibit *two* distinct mesh frequencies. Such systems are also free of the geometric constraint, $T_r = T_s + 2\,T_p$, imposed by the use of a ring.

Two issues of *assembly phase* must be addressed. The "outer" mesh between the ring and planets may exhibit N_{outer} possible assembly phases (for each planet gear) while the mesh between the planets and Sun gear may exhibit N_{inner}. In the spirit of Equation (1), N_{outer} is recognized as the largest (integer) common factor of T_r and T_p, while N_{inner} is recognized as the largest (integer) common factor of T_s and T_p. This allows the inner and outer mesh assembly phase passage frequencies to be written in the manner of Equation (5).

$$f_{\text{outer AP}} = \frac{f_{\text{mesh}}}{N_{\text{outer}}} \tag{13}$$

$$f_{\text{inner AP}} = \frac{f_{\text{mesh}}}{N_{\text{inner}}} \tag{14}$$

In like manner, the system will exhibit *two* hunting tooth-frequencies, one for the outer mesh and one for the inner mesh. These frequencies are determined as in Equation (6), and we find:

$$f_{\text{outer HT}} = \frac{N_{\text{outer}}}{T_r T_p} f_{\text{mesh}} \tag{15}$$

$$f_{\text{inner HT}} = \frac{N_{\text{inner}}}{T_s T_p} f_{\text{mesh}} \tag{16}$$

All prior comments regarding the use of these five characteristic frequencies apply to the epicyclic gear drive as well. Note, however, that this system exhibits N "mesh points" (one for each planet) and that these points rotate at f_{out}. This gives rise to additional terms at $N f_{\text{out}}$ and $f_{\text{mesh}} \pm N f_{\text{out}}$.

Baring the Bearing

Rolling element bearings exhibit a striking geometric similarity to the epicyclic gear train just discussed. Figure 10 illustrates the schematic diagram of a single-row ball bearing. The relative motions in this system are analogous to those of the planetary gear system with the ratios between elements being determined by the *rolling diameters* of the components.

N balls of diameter d are held between the *inner race* and the *outer race* on a *pitch diameter D*. The inner race is pressed on the borne shaft and rotates with it; the outer race is retained motionless by the stationary bearing housing. The spacing between the balls is held constant by a pressed *cage* which allows the balls to spin freely and is, itself, free to precess relative to the races. The cage and races are most commonly designed to *incline the ball spin axes*; this is done to allow the

Table 2. Analysis of epicyclic motion by superposition of two input motions (in blue).

Motion of:	Planet Gears	Sun Gear (Input Shaft)	Gear Carrier (Output Shaft)	Ring Gear (Housing)
(1) lock carrier, rotate planet	β	$\frac{-T_p}{T_s}\beta$	0	$\frac{-T_p}{T_r}\beta$
(2) lock train, rotate housing	$\frac{-T_p}{T_r}\beta$	$\frac{-T_p}{T_r}\beta$	$\frac{-T_p}{T_r}\beta$	$\frac{-T_p}{T_r}\beta$
(3) sum of motions	$\frac{(T_r-T_p)}{T_r}\beta$	$-\frac{(T_pT_r+T_pT_s)}{T_sT_r}\beta$	$\frac{-T_p}{T_r}\beta$	0

Table 3. Epicyclic motions normalized to one rotation of the output.

Normalized Motion of:	Planet Gears	Sun Gear (Input Shaft)	Gear Carrier (Output Shaft)	Ring Gear (Housing)
(1) lock carrier, rotate planet	$\frac{-T_r}{T_p}$	$\frac{T_r}{T_s}$	0	–1
(2) lock train, rotate housing	1	1	1	1
(3) sum of motions	$1-\frac{T_r}{T_p}$	$1+\frac{T_r}{T_s}$	1	0

bearing to react to a shaft-axial force. The inclination of the spin axis is defined by the (small) *contact angle* α.

The tolerances of a ball bearing are tightly controlled so that the balls must roll on the races, rather than slipping. From inspection of the geometry in Figure 10, we can recognize that the balls roll about an inner diameter of $D - d\cos\alpha$, and within an outer diameter of $D + \cos\alpha$. Knowing the diameter ratios allows us to analyze the bearing by superposition in exactly the same fashion as previously discussed.

Table 4 presents the tabular analysis of the bearing. In the top row, the cage is held stationary, while both the inner and outer races are left free to rotate. A ball is rotated through an arbitrary angle β causing the outer race to rotate in the same direction and the inner race to rotate with opposite sense. In the second row, all bearing elements are locked together and the bearing is rotated in a direction opposite the first input until the outer race is restored to its original position. The third row presents the sum of these two motions and provides the positions of the cage and inner race.

All pertinent motions are then normalized to one rotation of the *inner race* (shaft). This step is different from the gear analysis, where rotations were normalized upon the *carrier* which is synonymous with the bearing's *cage*. From the entries of Table 4 we can determine the rotational speeds of *ball spin* and *cage precession* relative to shaft speed. Specifically:

$$f_{\text{ball spin}} = \frac{D^2 - d^2\cos^2\alpha}{2Dd} f_{\text{shaft}} \tag{17}$$

and:

$$f_{\text{cage}} = \frac{D - d\cos\alpha}{2D} f_{\text{shaft}} \tag{18}$$

These frequencies of component motion combine in various fashions when an element of the bearing becomes flawed. As an example, consider a pit or spall on the outer race. Such a flaw causes an impact each time a ball crosses it. Hence there will be N impacts for every revolution of the cage. Since the impacts are of short duration, they will exhibit many harmonics. Thus we can identify an *outer race fault* by the presence of spectral peaks at:

$$f_{\text{Outer Race Fault}} = k N f_{\text{cage}} \quad k = 1,\ 2,\ 3 \ldots \text{(harmonics)} \tag{19}$$

A fault on a single ball will alternately strike the inner and outer races. This will give rise to periodic forces at twice the ball spin frequency. Since each impact is a brief duration event, the spectrum will contain many harmonics of $2\, f_{\text{ball spin}}$. Further, the contact points (and therefore the force direction) rotate at the cage precession frequency, following a single ball. Hence a *ball fault* will exhibit vibration peaks at frequencies of:

$$f_{\text{Ball Fault}} = 2\, k\, f_{\text{ball spin}} \pm f_{\text{cage}} \quad k = 1,\ 2,\ 3 \ldots \text{(harmonics)} \tag{20}$$

From the first row and second column of Table 4 we can deduce that a single ball contacts a fixed point on the inner race with a frequency of :

$$f_{\text{IR contact}} = \frac{d}{D - d\cos\alpha} f_{\text{ball spin}} = \frac{D + d\cos\alpha}{2D} f_{\text{shaft}} \tag{21}$$

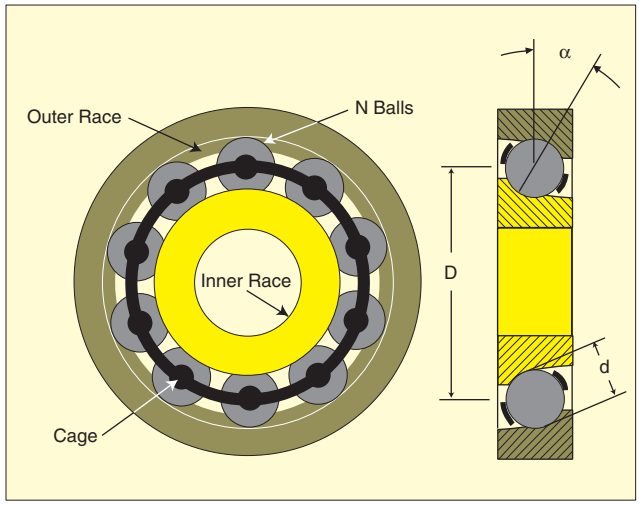

Figure 10. Geometry of a ball bearing is defined by Pitch Diameter, D, Ball Diameter, d, and Contact Angle, α. The rolling elements form an epicyclic system similar to that of Figure 8 with a Sun gear diameter = $D - d\cos\alpha$, a planet diameter = d and a ring diameter = $D + d\cos\alpha$.

A defect on the inner race will be impacted by each of the N balls in sequence. Each impact will be brief, leading to a periodic force rich in harmonics. Since the fault location rotates with the shaft, the force direction rotates at f_{shaft} and the resulting *inner race fault* exhibits spectral peaks at:

$$f_{\text{Inner Race Fault}} = k N F_{\text{IR contact}} \pm f_{\text{shaft}} \quad k = 1,\ 2,\ 3 \ldots \text{(harmonics)} \tag{22}$$

It is not uncommon to be faced with an operating machine for which bearing data are not immediately available. Reasonable "ball park" *estimates* of bearing fault-frequency can be formed by assuming α equal to 0° and d/D equal to 0.25. This results in the approximations:

$$f_{\text{Ball Fault}} \cong (3.75\, k \pm 0.375) f_{\text{shaft}} \quad k = 1,\ 2,\ 3 \ldots \text{(harmonics)} \tag{23}$$

$$f_{\text{Inner Race Fault}} \cong (0.625\, k N \pm 1) f_{\text{shaft}} \quad k = 1,\ 2,\ 3 \ldots \text{(harmonics)} \tag{24}$$

$$f_{\text{Outer Race Fault}} \cong 0.375\, k N f_{\text{shaft}} \quad k = 1,\ 2,\ 3 \ldots \text{(harmonics)} \tag{25}$$

Should a *race fault* be evident, it is likely to "count the balls" for you by disclosing either $\cong 0.375\, N f_{\text{shaft}}$ or $\cong 0.625\, N f_{\text{shaft}}$ as the peak-spacing of the $k N f_{\text{shaft}}$ "clusters". A *single ball* fault will not disclose how many balls are in the bearing.

Dip in the Data, Bathe in the Waterfalls

Our attention returns to the small speed-reducer and the vibration signatures it exhibits. Figure 11 shows this gearmotor mounted in a simple test fixture. An accelerometer monitors case vibration over the end of the transfer shaft (refer to Figure 2) and we will focus on observations made with this sensor. Our test rig permits fixed and variable speed operation. All measurements are made with the gearbox *unloaded* (and

Table 4. Analysis of epicyclic bearing motion by superposition of two input motions (in blue).

Motion of:	Balls	Inner Race (Shaft)	Cage	Outer Race (Bearing Housing)
(1) lock cage, rotate ball	β	$\frac{-d}{D - d\cos\alpha}\beta$	0	$\frac{d}{D + d\cos\alpha}\beta$
(2) lock, rotate outer race	$\frac{-d}{D + d\cos\alpha}\beta$	$\frac{-d}{D + d\cos\alpha}\beta$	$\frac{-d}{D + d\cos\alpha}\beta$	$\frac{-d}{D + d\cos\alpha}\beta$
(3) sum of motions	$\frac{D + d\cos\alpha - d}{D + d\cos\alpha}\beta$	$\frac{-2dD}{D^2 - d^2\cos\alpha}\beta$	$\frac{-d}{D + d\cos\alpha}\beta$	0

Figure 11. Gearmotor in test fixture. PCB 352C67 accelerometer monitors case vibration over the worm gear end of the transfer-shaft. Omron EE-SPX301 IR diode/receiver monitors output shaft speed, viewing disk with one or eight holes. Other sensors measure motor-current, radial magnetic flux and local sound pressure. Variable speed operation in both directions is accommodated.

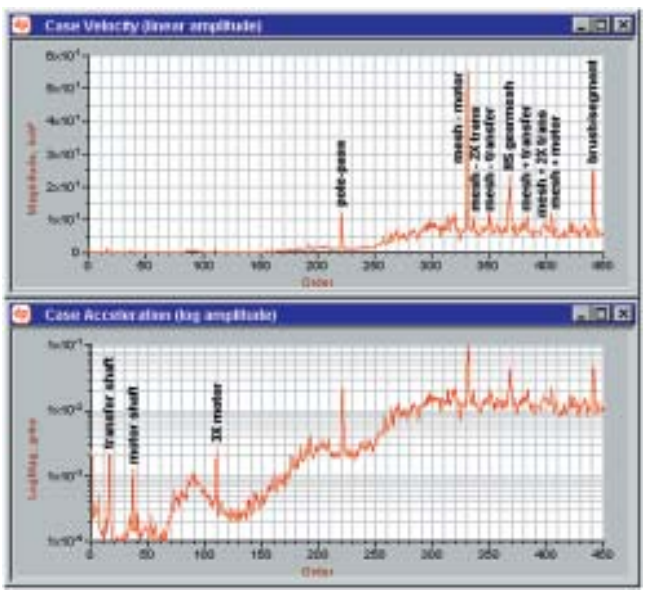

Figure 12. Typical order-normalized case vibration signatures. Upper trace presents velocity spectrum with linear IPS (peak) vertical axis. Lower trace shows corresponding g (RMS) acceleration spectrum with a logarithmic vertical axis. Horizontal axes are in orders of the output-shaft speed. Source of dominant tones are marked (compare with list of Table 1). Note that the dominance of order 331.2 (Mesh - Motor) and the appearance of order 10.4 (3X Motor Shaft speed) qualify as surprises.

unlubricated!) in an attempt to make its inner workings more obvious to external measurement.

Figure 12 illustrates order-normalized spectra (see sidebar) spanning the expectations of the "shopping list" of Table 1. Two presentations of the same measurement are made. The upper trace shows the (linear) velocity spectrum while the lower trace presents acceleration on a logarithmic axis. The mechanical source identification of each peak is labeled.

Velocity measurements relate well to accepted machinery health criteria. Clearly, the 0.55 IPS peak in this spectrum would qualify a process machine as a 'hot' maintenance candidate! Note that this peak value occurs at order 331.2 which appears on our shopping list as the lower motor-speed sideband of the primary (high-speed) gearmesh. However the corresponding *upper* motor-speed sideband (at order 404.8) is certainly not symmetric in amplitude; it is only 20% as large. Further, this "sideband" is considerably greater than the high-speed gearmesh "carrier" component at order 368. This qualifies as a surprise!

A plausible explanation for this asymmetry is that the gearmesh is experiencing some combination of both *amplitude modulation and frequency modulation* at the motor-shaft speed. Appropriate phasing between these mechanisms can accentuate one sideband and suppress the other. However, order 331.2 also corresponds to the ninth harmonic of motor

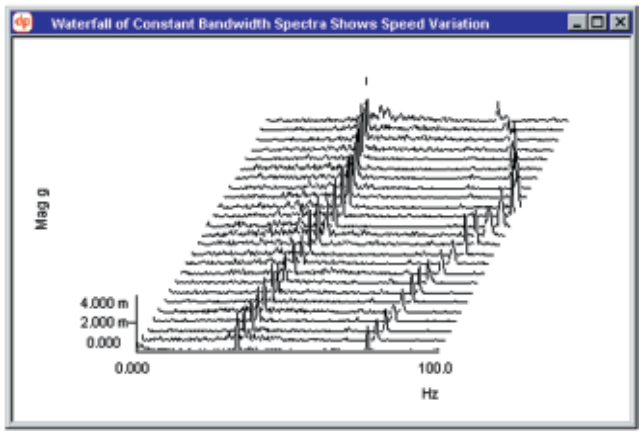

Figure 13. Waterfall of constant frequency-span acceleration spectra during variable speed operation shows low frequency (DC -100 Hz) case vibration is dominated by two tones that vary in frequency proportional to shaft running-speed. The amplitude axis presents g (RMS) with linear scaling; the traces are separated by 8 seconds with the oldest trace "at the top".

speed and other explanations are possible.

The high-speed gearmesh is also symmetrically bounded by ±16 order and ±32 order sidebands indicating modulation at the transfer-shaft speed and its second harmonic. These terms are of much lower amplitude and exhibit the anticipated symmetry associated with simple amplitude modulation. The expected magnetic pole-passage frequency (6× motor speed) and brush/commutator-segment contact rate (12× motor speed) are also present at orders 220.8 and 441.6, respectively.

The (lower) acceleration trace is shown on a log axis, so that amplitudes spanning a 1000:1 range may be seen. This compression emphasizes the low amplitude features not discernible in a linear display. All features identified from the velocity spectrum show up clearly in this acceleration trace. Additionally, peaks at the transfer-shaft (order 16) and motor-turning (order 36.8) speeds may be clearly seen. Note that an additional (minor) "surprise" is found in this spectrum, the peak at three times the motor shaft speed.

Clearly, presenting the measurement on an order-normalized basis ma When a machine operates at a *truly* steady speed, the conversion from a conventional "fixed bandwidth" spectrum to an order-normalized display seems trivial. However, nothing mechanical is ever *really* steady in its operating speed. Even electrical power-generation systems that maintain line frequency to a tolerance of *degrees per day* exhibit instantaneous speed variations that can "blur" spectral orders in an averaged measurement made with constant bandwidth.

Consider the more extreme speed variation shown in Figure 13. Here a series of fixed bandwidth spectra are presented in a *waterfall* format. Each spectrum is separated from its neighbor by a fixed time increment so that the waterfall presents a time/frequency/amplitude topology. In this figure, the frequency range encompasses the transfer-shaft (order 16) and motor-shaft (order 36.8) speeds while the machine is varied up and down between 125 and 160 RPM. Linear amplitude scaling of the case acceleration is shown. Certainly, any attempt to ensemble-average these spectra would result in a "blurred" picture of the machine's activity.

The same collection of spectra is presented as a *spectrogram* in Figure 14. Here, the amplitude is encoded by color (scale to right), frequency is horizontal and time is vertical. The time/frequency "tracks" of the 16^{th} and 36.8^{th} order components are clearly visible.

Figure 15 presents a similar analysis using order-normalized spectrum measurement. In this presentation, the activity at each order maintains a fixed horizontal axis position, even though the machine speed is varying. The *amplitude* at each order can vary as the machine speed changes, but the order maintains a fixed horizontal location in each spectrum. Hence, ensemble averaging can be applied to such spectra without fear

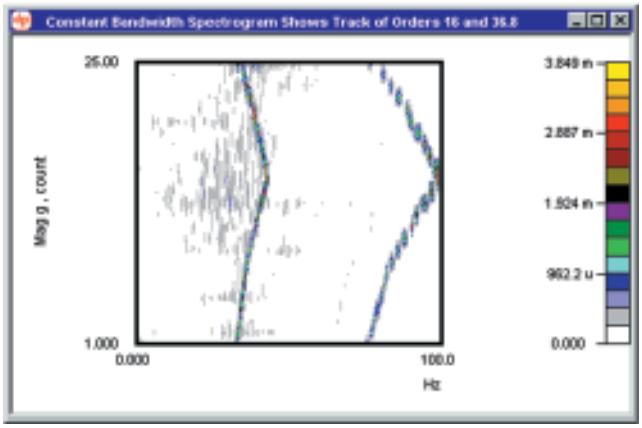

Figure 14. Spectrogram display presents the same data as the waterfall of Figure13 in an alternate format. Here, the acceleration level is represented by color. This presentation emphasizes the time/frequency track of dominant tones. Those shown here correspond to orders 16 (transfer-shaft speed) and 36.8 (motor speed).

of a "blurred" result.

The amplitude variation in the 36.8 order can be seen from the red cursor line following that order. These data are presented more clearly in the companion *order track* plot that presents 36.8th order acceleration versus output shaft RPM.

Tachs can be Tacky and Taxing

As discussed in the *Law and Order Normalization* sidebar, a tachometer signal is used to synchronize the analyzer to a rotating machine for order-analysis. The sample rate is derived as a multiple of the frequency of this pulse train. Clearly, any frequency-multiplication process must make assumptions about the instantaneous speed *between* tach pulses. For this reason, it is good practice to apply the tachometer at the "high speed" end of a multi-shaft gear system. Unfortunately, this is not always possible. As in our example machine, the low-speed process output is frequently the most accessible (often only!) place where train speed can be measured.

One solution to this difficulty is to use a multi-pulse per revolution tachometer such as a precision *shaft encoder*. Often, the teeth of a passing gear may be viewed with a shaft probe rather than simply viewing a keyway. These are perfectly valid approaches that minimize the amount of "mathematical" frequency multiplication required. All things being equal, performing an order-normalization with a high number of pulses/revolution *mechanically* sensed from the machine is always preferable.

However, things are not always equal (pun intended)! "Home grown" multi-pulse per revolution tachometers frequently compromise the analysis because the multiple targets are ***not*** equally separated. Unless you are convinced that the targets are precisely spaced (as in a commercial encoder) be alert for tachometer-induced artifacts.

Consider the two tachometer target wheels shown in Figure 16. These were produced in a "Scottish machine shop" (one where the only tools are a drill press and a file). While the 8/rev unit on the right appears reasonably symmetric, it actually has enough variation in the target-hole locations to compromise an analysis.

When this unit is turned at constant velocity, the resulting tach pulses produced by the infrared interrupter module seen in Figure 11 are not equally spaced; they "jitter" in time. That is, the tachometer signal is *frequency modulated*. In contrast, the single target disk *must* produce a constant rate output (as long as it is firmly fixed to a shaft that cannot move laterally).

Consider the comparison of Figure 17. In the top figure, the auto spectrum of the 1/rev tachometer signal is shown. This measurement was made using constant-bandwidth analysis with the machine running at a constant speed. The lower trace repeats this measurement with the 8/rev disk installed. For visual simplicity, the frequency axes have been scaled to read

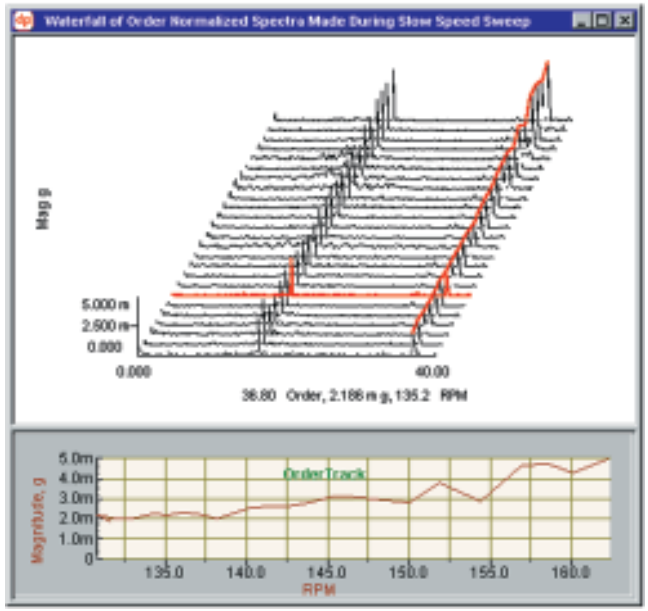

Figure 15. Waterfall of order-normalized acceleration spectra during variable speed operation. The horizontal axis spans 40 orders of output shaft speed, which approximates the range of frequency span in Figures 13 and 14. Note that the 16th and 36.8th order "tracks" become straight lines. The companion plot presents the variation in vibration amplitude at the 36.8 order (motor speed) with changing RPM.

Figure 16. Two tachometer wheels used in rig testing. The wheel on the left provided one pulse per output-shaft rotation while that on the right provided eight. Seemingly minor machining imperfections degraded analysis when the 8/rev unit was employed. This is a common problem in "home grown" multi-pulse per revolution tachometers.

in orders of the shaft speed.

The spectrum of the 1/rev tach is exactly as anticipated. There are peaks at the shaft-turning frequency and its harmonics. Since the output of the interrupter is a TTL logic signal, these harmonics are distributed with $\sin(x)/x$ amplitude. Each peak is relatively narrow and the "noise floor" is about 40 dB (100:1) below the fundamental peak. We would anticipate the 8/rev spectrum to have the same form with its fundamental appearing eight times as high.

Instead, we find the 8/rev tach disk produces a strong series of 1/rev spaced *sidebands*, symmetrically distributed about the 8/rev fundamental. This is the classic spectral form of a frequency modulation. The sidebands are significant, starting from only 22 dB (12.6:1) below the fundamental.

Figure 18 illustrates a 40 order normalized analysis made of the acceleration signal using the 1/rev tachometer with the machine operating at constant speed. This low frequency study provides clean definition of the 16th order transfer-shaft and 36.8th order motor-speed components. It also shows virtually every order of the output shaft as a clean and discernible feature.

The same analysis is repeated in Figure 19 using the 8/rev tach disk. Note the difference in form. While the 16th and 36.8th order components are properly placed, the lower amplitude terms are severely distorted. As an example, note the first three

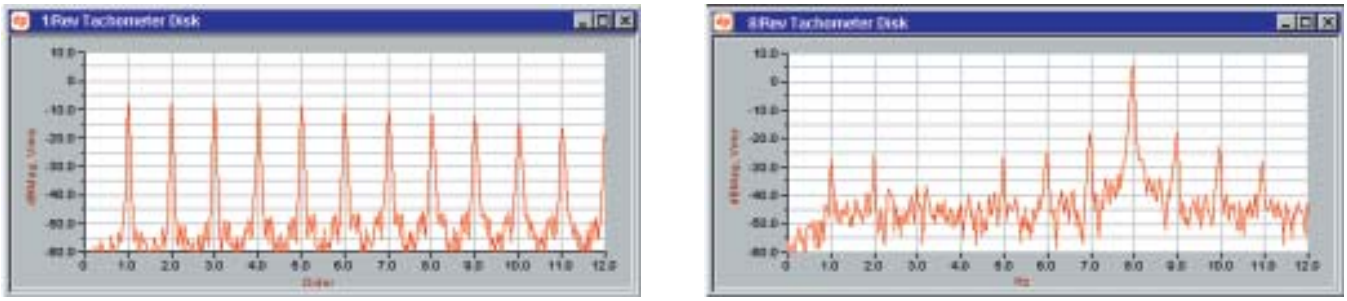

Figure 17. Comparison of spectra of the tachometer signals, 1/rev disk left, 8/rev right. The machine was run at constant speed and spectra were measured using normal constant-bandwidth analysis. The frequency axes have been normalized to orders by dividing by the dominant tachometer frequency. While the left plot shows some minor evidence of machine-speed variation, the right plot exhibits rampant 1/rev sidebands about the 8/rev fundamental. This indicates the 8/rev tachometer pulse train is frequency modulated by imperfections in the placement of the eight target holes (see Figure 16).

peaks which are shown *between* integer multiples of the shaft speed.

Precise order-normalized measurements require precise speed transduction. Use your spectrum analyzer to validate the performance of your tachometer before using it as the reference for more involved studies. Whenever feasible, verify a multi-pulse tachometer by comparing its output against a 1/turn signal experiencing the same machine-speed variability.

Closure

All measurements presented in this article were made with the new multichannel Data Physics SignalCalc® 620 VXI system illustrated in Figure 20. Data Physics also offers similar analytic capabilities in more compact 430 (ISA card) and ACE

Law and Order Normalization

Order-normalized spectrum measurements may be made by several techniques. When the studied machine operates at a constant speed, an ordinary spectrum analysis may be made and the frequency axis may be scaled to *orders* by dividing by the shaft running-speed. When the machine speed is more agile, specific hardware and software must be employed to *sample the measured signals a constant number of times per shaft revolution*, rather than sampling on a constant time-interval basis.

In a fixed-bandwidth operation, an analyzer collects N successive samples from an analog time-history at a sample rate f_s. The analog signal is pre-filtered by a low-pass *anti-aliasing* filter set to the desired analysis frequency range, F_{span} and the sample rate is set to $k\,F_{span}$, where k is a constant specific to the analyzer. Each captured time-history is transformed to yield a spectrum. The following spans and resolutions result:

$\Delta t = 1/f_s = 1/(kF_{span})$ = time between adjacent time points (S)

$T_{span} = N\,\Delta t$ = duration of each time capture or memory load period (S)

$\Delta F = 1/T_{span}$ = difference between adjacent frequency points (Hz)

$F_{span} = N\,\Delta F/k$ = frequency range presented (Hz)

In order-normalized analysis, both the frequency range and sample rate must *vary* in proportion to the machine speed. This is accomplished by measuring the shaft speed with a tachometer and deriving a sample rate equal to $k\,O_{span}$ times the shaft speed. O_{span} is the *maximum* number of shaft-speed orders (multiples) to be measured in a spectrum. The anti-aliasing filter must constantly adjust to limit the incoming signal bandwidth to O_{span} times the shaft-turning frequency. This results in the following spans and resolutions:

$\Delta R = 1/f_s = 1/(kO_{span})$ = shaft-angle between adjacent signal samples (Revolution)

$R_{span} = N\,\Delta R$ = number of turns in each memory capture (Revolution)

$\Delta O = 1/R_{span}$ = difference between adjacent order points (Order)

$O_{span} = N\,\Delta O/k$ = order span presented (Order)

Typical analyzers (of either FFT or *time compression* type) require between 2.56 and 4 samples *per maximum order spanned*. This is the same k multiple relating the analyzer's sample-rate to the frequency band studied in normal fixed-bandwidth analysis. The exact numeric value is determined by the analyzer's design specifics.

The functional block diagram of a hybrid *Tracking Adapter* is shown below. Tracking adapters have been supplanted by more modern methods, but many of these "basic workhorses" remain in daily service. This figure illustrates several basic points of technology worthy of discussion.

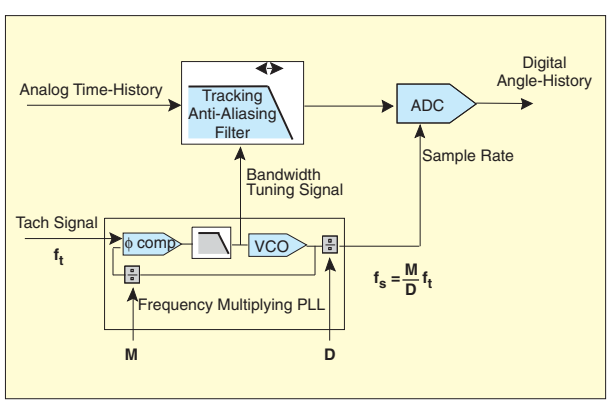

The tracking adapter performs two related functions. It derives a sample-rate proportional to shaft speed from a reference tachometer signal (a once-per-turn pulse train), and it provides an anti-aliasing filter with bandwidth instantaneously adjusted in proportion to the shaft speed. At the heart of this instrument is a circuit called a phase-locked loop (PLL) which is involved in both functions.

The tachometer typically provides a single pulse-per-revolution; we require many pulses-per-revolution to accurately define each turn. The necessary frequency multiplication is accomplished by the PLL, a servo loop which forces a local voltage controlled oscillator (VCO) to produce a pulse train at (integer) M times the tachometer frequency; this is rate divided by integer D and applied to a spectrum

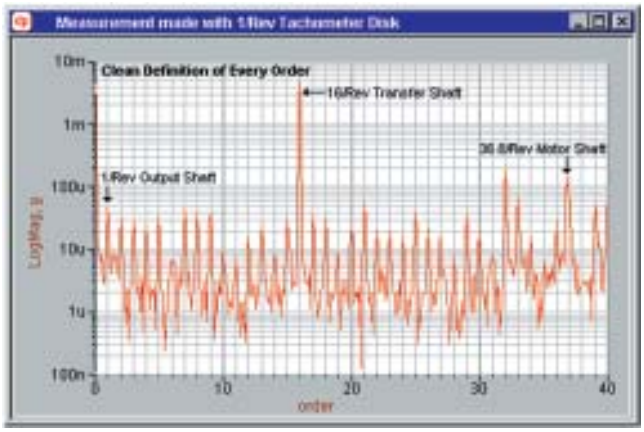

Figure 18. Order-normalized acceleration spectrum measured using 1/rev tachometer disk shown in Figure 16. Machine was run at constant speed and 50 spectra averaged. This plot spans 40 orders with a horizontal resolution of 0.1 orders (each spectrum was computed from a 10 output-revolution capture). The spectrum is dominated by the tones at transfer-shaft and motor-shaft speeds. Note, however, that virtually every multiple of the output-shaft speed (1/rev) can be seen clearly in this plot.

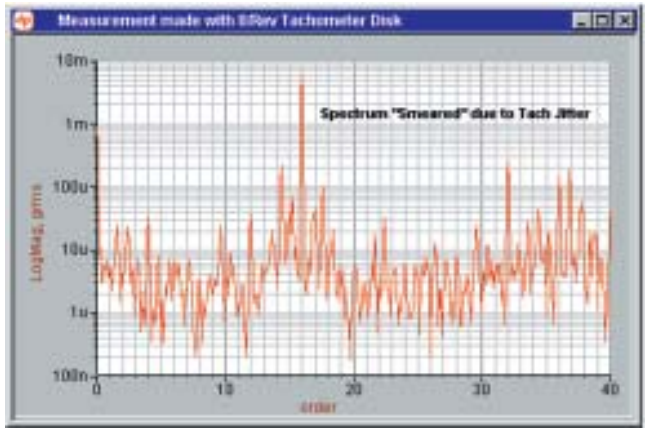

Figure 19. Repeat of the analysis of Figure 18 using the 8/rev tachometer disk. Note the distortion, blurring and misplacement of low amplitude terms. As an example, the first three peaks are no longer seen as multiples of 1/rev; they appear at non-integer orders! Poor precision in machining a multiple-target tachometer can compromise the precision and dynamic range of an order-normalized analysis. Your spectrum analyzer can identify the frequency modulation introduced by imprecise tachometer targets.

analyzer's ADC as the sample rate. Thus selecting the appropriate integers M and D allows (limited) setting of the number of samples per revolution.

Within the phase-locked loop, an analog voltage proportional to frequency is developed. This signal is used to "tune" a voltage-controlled low-pass filter, the anti-aliasing filter applied to the measured vibration signal. Thus the upper frequency of this filter is caused to track the sample rate (and thus the shaft speed) providing variable frequency alias rejection as RPM varies.

Tracking adapters made order-normalized spectrum analysis possible; they also exhibited several shortcomings. Since the PLL only "updates" at each tach-pulse arrival, the circuit "assumes" the shaft to rotate with constant angular velocity between pulses. This is a poor match for important run-up examinations. In general, error in sample placement increases throughout the revolution rather than being uniformly distributed throughout the measurement.

A filter within the PLL provides some "memory" to stabilize the circuit between tachometer pulses. This loop filter seriously reduces the circuit's ability to follow rapid speed changes accurately. Such "slew-rate" limiting becomes more pronounced at high M values required to track a large number of orders.

The tunable anti-aliasing filter limits dynamic range as it is not possible to build a variable frequency analog filter with anywhere near the same transition-band steepness as can be done in fixed-frequency designs. Alternative technologies incorporating charged-coupled devices have proven even less effective in this regard.

Tracking adapters are hardware intensive and thus expensive. The added weight and volume of "another instrument" is never appreciated when making field measurements.

Modern analyzers employ a different approach, one which adds very little additional hardware to the instrument. This digital re-sampling process overcomes all of the shortcomings common to tracking adapters and provides accurate, resolute analysis with deep dynamic range for all machines including those that accelerate rapidly. The following figure illustrates the re-sampling process.

The vibration signal is sampled by an ADC running at a *constant* sample rate and is protected by a standard *fixed-frequency* anti-aliasing filter. The bandwidth of this filter, F_{span}, is selected such that . . .

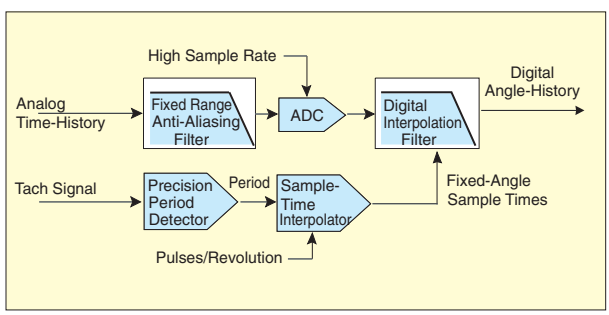

$$F_{span} \geq \mathrm{RPM}_{max} \times O_{span} / 60$$

where RPM_{max} is the maximum machine shaft speed anticipated and O_{span} is the maximum order of shaft rotation to be analyzed. The sample-rate f_s is set to a deliberately high value with regard to the input filter (f_s = 5.12 F_{span} being typical).

The resulting over-sampled digital time history is passed to the input memory of a digital amplitude-interpolation filter. The output of this low-pass filter is sampled at a fixed number of times per revolution. These sample times are ***not*** uniformly spaced in time. Rather, each sample is taken at a time corresponding to a shaft rotation of ***dR*** from its predecessor. These fixed-angle sample times are computed from successive periods of the tachometer signal.

The tachometer pulse train is applied to a precise timing circuit which measures the period between pulses. These periods are sent to an interpolation module which computes the appropriate times at which to sample the interpolation filter's output. The sample times between tachometer pulses are computed by a curve-fitter which assumes the shaft experiences *constant acceleration* between pulses. This module accepts a **pulse-per-revolution** argument, allowing the use of one or more equally spaced tachometer pulses per shaft rotation.

The resulting digital angle-history is presented for subsequent FFT and average processing. The interpolation filter introduces a slight processing delay between the ADC input and the presentation of the angle-history. However, this delay affects all channels identically and the process proceeds in real-time without compromise.

Figure 20. The SignalCalc® 620 Dynamic Signal Analyzer by Data Physics Corporation uses HP VXI frames and modules to provide a full-function FFT/Octave-Band/Order-Tracking analyzer with up to 128 channels of input. A broad range of configurations is offered including choice of in-frame or external CPU, any mix of HP E1432A, HP E1433A and HP E1434A modules, real-time recording, ActiveX Connectivity and MIMO processing. All configurations respond to the simple, consistent SignalCalc interface used in all Data Physics analyzers. The software is compatible with Windows® NT, 95 and 98 operating systems.

(PCMCIA module) systems of lower channel count.

We have introduced some recommended work methods for machinery diagnosticians with particular emphasis on being prepared to appreciate and critique measurement results. Basic signature frequencies for bearings and gears have been developed and their utility visualized through experiment. Theory and implementation of order-normalized spectrum analysis have been reviewed. Certain frailties of tachometer systems have been brought to your attention. In short, this has been a very full lecture. Your quiz will come tomorrow, in field. Good luck and Class Dismissed! SV